Int. J. Pure Appl. Sci. Technol., 24(1) (2014), pp. 18-30

International Journal of Pure and Applied Sciences and Technology

ISSN 2229 - 6107

Available online at ***www.ijopaasat.in***

Research Paper

Reflection and Transmission of Elastic Waves at an Imperfectly Bonded Interface between an Elastic Solid and a Viscoelastic Porous Solid Saturated by Viscous Liquid

Baljeet Singh[1,*] and Surjeet Singh[1]

[1] Department of Mathematics, Post Graduate Government College, Sector 11, Chandigarh, India

* Corresponding author, e-mail: (bsingh@gc11.ac.in)

(Received: 6-8-14; Accepted: 26-8-14)

Abstract: *The present paper is concerned with a problem on reflection and transmission of elastic waves at an imperfectly bonded interface between an elastic solid and a viscoelastic porous solid saturated by viscous liquid. The appropriate potential functions for reflected and transmitted waves satisfy the required boundary conditions at the interface. The relations between amplitude ratios of different reflected and refracted waves are obtained for incidence of P and SV waves. The amplitude ratios of various reflected and refracted waves are computed for a particular model. The effect of imperfect boundary is observed on these amplitude ratios.*

Keywords: Viscoelastic porous solid, Reflection and transmission, Imperfect boundary, Amplitude ratio.

1. Introduction

Information regarding the composition and state of deep interior can be obtained from observed attenuation of the seismic wave in the earth. The attenuation of seismic waves cannot be explained by considering the earth to be an elastic solid. Viscoelasticity is an important property of many rocks in the crust, which is a major cause of seismic attenuation. A viscoelastic solid permeated by pores and fractures and saturated with viscous fluid becomes a more realistic model in the presence of porosity for sedimentary or reservoir rocks.

Biot (1956a) studied the propagation of the plane harmonic seismic waves in liquid saturated porous solids. Biot (1956b) developed the equations for the deformation of a viscoelastic porous solid containing a viscous fluid under the most general assumptions of anisotropy. Biot (1962) presented

the mechanics of deformation and acoustic propagation in porous media, where liquid-solid medium is considered as a complex physico-chemical system with resultant relaxation and viscoelastic properties. Sharma and Gogna (1991) studied the seismic wave propagation in a viscoelastic porous solid saturated by viscous liquid. Vashishth and Sharma (2008) discussed the wave propagation in a medium considered as a viscoelastic, anisotropic and porous solid frame such that its pores of anisotropic permeability are filled with a viscous fluid. Recently, Sharma (2012) studied the propagation of Rayleigh waves on the stress-free surface of a viscoelastic porous solid saturated with viscous fluid.

In the present paper, the reflection and transmission of elastic waves is studied at an imperfect boundary between an elastic solid and a viscoelastic porous solid saturated by viscous liquid. For incidence of *P* and *SV* waves, the amplitude ratios of various reflected and refracted waves are computed for a particular model. The effect of imperfect boundary is shown graphically.

2. Basic Equations

Following Biot (1956b, 1962), the governing equations of viscoelastic porous solid saturated by viscous liquid are

$$\tau_{ij} = 2\mu^* e_{ij} + \left[\left(\lambda^* + \alpha^{*2} M^*\right) e + \alpha^* M^* \xi\right]\delta_{ij},\ p_f = -\alpha^* M^* e - M^* \xi, \tag{1}$$

$$\mu^* \nabla^2 \vec{u} + \left(\lambda^* + \mu^* + \alpha^{*2} M^*\right)\nabla e + \alpha^* M^* \nabla \xi = \frac{\partial^2}{\partial t^2}\left(\rho \vec{u} + \rho_f \vec{w}\right), \tag{2}$$

$$\nabla\left(\alpha^* M^* e + M^* \xi\right) = \frac{\partial^2}{\partial t^2}\left(\rho_f \vec{u} + m\vec{w}\right) + \frac{\eta}{\chi}\frac{\partial \vec{w}}{\partial t}, \tag{3}$$

where $e_{ij} = \frac{1}{2}\left(u_{i,j} + u_{j,i}\right)$ is strain tensor, $e = div\ \vec{u}$, $\xi = div\, \vec{w}$ are the dilatations, τ_{ij} is stress tensor, p_f is liquid pressure, $\vec{w} = \beta\left(\vec{U} - \vec{u}\right)$ represents the flow of liquid relative to the solid measured in terms of volume per unit area of the bulk medium, λ^*, μ^* are Lame's constants for the solid, ρ is mass density of the bulk material, ρ_f is mass density of liquid, *m* is Biot's parameter which depends upon porosity β and ρ_f, η is pore fluid viscosity, and χ is permeability. α^* and M^* are the elastic coefficients related to the coefficient of fluid content γ^*, unjacketed compressibility δ^* and jacketed incompressibility $K^*\left(= \lambda^* + \frac{2}{3}\mu^*\right)$ by $\alpha^* = 1 - \delta^* K^*$, $M^* = 1/\left(\gamma^* + \delta^* - \delta^{*2} K^*\right)$.

Following Sharma and Gogna (1991), in an unbounded viscoelastic porous solid saturated by viscous liquid, two dilatational waves of first and second kinds and one shear wave propagate. They also obtained the velocities v_j, $(j = 1,2)$ of dilatational waves and the velocity v_3 of shear wave as

$$v_j^2 = \frac{\lambda^* + 2\mu^*}{\rho_j^*},\ (j = 1,2),\ v_3^2 = \frac{\mu^*}{\rho_3^*}. \tag{4}$$

The components of displacement vectors are taken as

$$\vec{u} = (u, 0, w),\ \vec{\omega} = (U, 0, W),\ \vec{u}_e = (u_e, 0, w_e), \tag{5}$$

where

$$u = \frac{\partial \phi_{11}}{\partial x} + \frac{\partial \phi_{12}}{\partial x} + \frac{\partial \psi}{\partial z},\ w = \frac{\partial \phi_{11}}{\partial z} + \frac{\partial \phi_{12}}{\partial z} - \frac{\partial \psi}{\partial x},\ \psi = (-\vec{\psi}_1),$$

$$U = \mu_1 \frac{\partial \phi_{11}}{\partial x} + \mu_2 \frac{\partial \phi_{12}}{\partial x} + \alpha_0 \frac{\partial \psi}{\partial z},\ W = \mu_1 \frac{\partial \phi_{11}}{\partial z} + \mu_2 \frac{d\phi_{12}}{\partial z} - \alpha_0 \frac{\partial \psi}{\partial x},$$

$$u_e = \frac{\partial \phi_e}{\partial x} + \frac{\partial \psi_e}{\partial z},\ w_e = \frac{\partial \phi_e}{\partial z} - \frac{\partial \psi_e}{\partial x},\ \psi_e = (-\vec{\psi}_e),$$

$$\mu_j = \frac{\rho_f \alpha^* - \rho + (\lambda^* + 2\mu^*)/v_j^2}{\rho_f - \left(m + i\frac{\eta}{\omega\chi}\right)\alpha^*},\ (j = 1, 2),\ \alpha_0 = -\frac{\rho_f}{(m + i\eta/\omega\chi)}.$$

3. Reflection and Transmission

For incidence of *P* or *SV* wave, there will be reflected *P*, SV waves in elastic half-space and refracted dilatational waves and shear wave in viscoelastic porous solid as shown in Figure 1. The appropriate boundary conditions at an imperfectly bonded interface z = 0 between elastic solid and viscoelastic porous solid half-spaces are

$$(\tau_{zz})_{II} + (p_f)_{II} = K_n (w_I - w_{II}),\ (\tau_{xz})_{II} = K_t (u_I - u_{II}),$$

$$(\tau_{zz})_{II} + (p_f)_{II} = (\tau_{zz})_I,\ (\tau_{xz})_{II} = (\tau_{xz})_I,\ (p_f)_{II} = 0, \tag{6}$$

where K_n, K_t are the normal and transverse stiffness coefficients of a unit thin layer thickness with dimension Nm^{-3}.

The appropriate potentials in elastic half-space are

$$\phi_e = A_0 e^{i(kx - d\alpha z - \omega t)} + A_1 e^{i(kx + d\alpha z - \omega t)}, \tag{7}$$

$$\psi_e = A_0^* e^{i(kx - d\beta z - \omega t)} + A_2 e^{i(kx + d\beta z - \omega t)}, \tag{8}$$

where $d\alpha = p.v.\left\{\left(\frac{\omega}{\alpha}\right)^2 - k^2\right\}^{\frac{1}{2}}$, $d\beta = p.v.\left\{\left(\frac{\omega}{\beta}\right)^2 - k^2\right\}^{\frac{1}{2}}$.

The appropriate potentials in viscoelastic porous solid half-space are

$$\phi_{11} = B_{11} e^{(-\vec{A}_{12} \cdot \vec{r})} \cdot e^{i(\vec{P}_{12} \cdot \vec{r} - \omega t)}, \tag{9}$$

$$\phi_{12} = B_{21} e^{\left(-\vec{A}_{22}\cdot\vec{r}\right)} \cdot e^{i\left(\vec{P}_{22}\cdot\vec{r}-\omega t\right)}, \tag{10}$$

$$\psi = C_{12} e^{-\left(\vec{A}_{32}\cdot\vec{r}\right)} \cdot e^{i\left(\vec{P}_{32}\cdot\vec{r}-\omega t\right)}, \tag{11}$$

where, the propagation vectors $\vec{P}_{ij}$ and attenuation vectors $\vec{A}_{ij}$ are defined by

$$\vec{P}_{ij} = k_{\mathrm{Re}}\hat{x} + (-1)^j d\upsilon_{i_{\mathrm{Re}}}\hat{z}, \quad \vec{A}_{ij} = k_{\mathrm{Im}}\hat{x} + (-1)^j d\upsilon_{i_{\mathrm{Im}}}\hat{z}, \quad \text{with } d\upsilon_i = p\cdot\upsilon\left(\frac{\omega^2}{\upsilon_i^2} - k^2\right)^{\frac{1}{2}}.$$

where $C_{12} = (-\vec{C}_1)_y$, $\vec{C}_1$ is arbitrary complex vector chosen such that $\nabla\cdot\vec{\psi} = 0$, k is an arbitrary complex number such that $k_{\mathrm{Re}} \geq 0$ to ensure propagation in the positive x-direction. The subscripts Re and Im denote the real and imaginary parts of the corresponding complex quantities. Following Borcherdt (1982), the displacement potentials given by (7) to (11) satisfy the boundary conditions for all values of *x* provided that

$$k = k_{\mathrm{Re}} = \frac{\omega\sin\theta_0}{\alpha \,or\, \beta} = \frac{\omega\sin\theta_1}{\alpha} = \frac{\omega\sin\theta_2}{\beta} = \left|\vec{P}_{12}\right|\sin\theta^*{}_1 = \left|\vec{P}_{22}\right|\sin\theta^*{}_2 = \left|\vec{P}_{32}\right|\sin\theta^*{}_3, \tag{12}$$

$$k_{\mathrm{Im}} = \left|\vec{A}_{j2}\right|\sin\left(\theta^*{}_j - \gamma_j\right), \ (j = 1,2,3) \tag{13}$$

which is the extension of Snell's law. We also obtain the following non-homogeneous system of five equations

$$\sum_{j=1}^{5} a_{ij} Z_j = b_i, \ (i = 1,2,..,5), \tag{14}$$

where

$$a_{11} = -i\ d\alpha K_n, \quad a_{12} = ik K_n,$$

$$a_{13} = -\left(d\upsilon_1\right)^2\left(H^* - \alpha^* M^*\right) - k^2\left(\lambda^* + \alpha^{*2} M^* - \alpha^* M^*\right)$$
$$-\mu_1\left(\alpha^* M^* - M^*\right)\left(k^2 + d\upsilon_1^2\right) - iK_n d\upsilon_1,$$

$$a_{14} = -\left(d\upsilon_2\right)^2\left(H^* - \alpha^* M^*\right) - k^2\left(\lambda^* + \alpha^{*2} M^* - \alpha^* M^*\right)$$
$$-\mu_2\left(\alpha^* M^* - M^*\right)\left(k^2 + d\upsilon_2^2\right) - iK_n d\upsilon_2,$$

$$a_{15} = kd\upsilon_3\left(-H^* + \lambda^* + \alpha^{*2} M^*\right) - ikK_n,$$

$$a_{21} = ikK_t, \quad a_{22} = id\beta K_t, \quad a_{23} = -2k\mu^* d\upsilon_1 - ikK_t,$$

$$a_{24} = -2k\mu^* d\upsilon_2 - ikK_t, \quad a_{25} = \mu^*\left[\left(d\upsilon_3\right)^2 - k^2\right] + id\upsilon_3 K_t,$$

$$a_{31} = -\lambda k^2 - (\lambda + 2\mu)(d\alpha)^2,$$

$$a_{32} = 2\mu kd\beta; \quad a_{33} = \left(H^* - \alpha^* M^*\right) dv_1^2 + k^2 \left\{\lambda^* + \alpha^{*2} M^* - \alpha^* M^* \left(1 - \mu_1\right) - \mu_1 M^*\right\}$$
$$+\mu_1 \left(\alpha^* M^* - M^*\right)\left(dv_1\right)^2,$$

$$a_{34} = \left(H^* - \alpha^* M^*\right)\left(dv_2\right)^2 + k^2 \left[\lambda^* + \alpha^{*2} M^* - \alpha^* M^* \left(1 - \mu_2\right) - \mu_2 M^*\right]$$
$$+\mu_2 \left(\alpha^* M^* - M^*\right)\left(dv_2\right)^2,$$

$$a_{35} = kdv_3 \left(H^* - \lambda^* - \alpha^{*2} M^*\right),$$
$$a_{41} = -2\mu kd\alpha, \quad a_{42} = -\mu\left\{\left(d\beta\right)^2 - k^2\right\}, \quad a_{43} = -2\mu^* kdv_1,$$
$$a_{44} = -2\mu^* kdv_2, \quad a_{45} = \mu^* \left\{\left(dv_3\right)^2 - k^2\right\},$$
$$a_{51} = 0, \quad a_{52} = 0,;$$

$$a_{53} = k^2 \left(\lambda^* + \alpha^{*2} M^* - \alpha^* M^*\right) + \left(\alpha^* M^* - M^*\right)\left\{\mu_1 k^2 + \mu_1 \left(dv_1\right)^2\right\},$$
$$a_{54} = k^2 \left(\lambda^* + \alpha^{*2} M^* - \alpha^* M^*\right) + \left(\alpha^* M^* - M^*\right)\left\{\mu_2 k^2 + \mu_2 \left(dv_2\right)^2\right\},$$
$$a_{55} = -kdv_3 \left(\lambda^* + \alpha^{*2} M^* - \alpha^* M^*\right).$$

(a) For incident *P* wave

$$b_1 = a_{11},\ b_2 = -a_{21},\ b_3 = -a_{31},\ b_4 = a_{41},\ b_5 = -a_{51},$$

and

$$Z_1 = \frac{A_1}{A_0},\ Z_2 = \frac{A_2}{A_0},\ Z_3 = \frac{B_{11}}{A_0},\ Z_4 = \frac{B_{21}}{A_0},\ Z_5 = \frac{C_{12}}{A_0},$$

are amplitude ratios of reflected *P*, reflected *SV*, refracted P_{12}, refracted P_{22} and refracted P_{32} waves, respectively.

(b) For incident SV wave,

$$b_1 = -a_{12},\ b_2 = a_{22},\ b_3 = a_{32},\ b_4 = -a_{42},\ b_5 = a_{52};$$

and

$$Z_1 = \frac{A_1}{A_0^*},\ Z_2 = \frac{A_2}{A_0^*},\ Z_3 = \frac{B_{11}}{A_0^*},\ Z_4 = \frac{B_{21}}{A_0^*},\ Z_5 = \frac{C_{12}}{A_0^*},$$

are amplitude ratios of reflected *P*, reflected *SV*, refracted P_{12}, refracted P_{22} and refracted P_{32} waves, respectively.

4. Numerical Results and Discussion

To compute reflection and transmission coefficients, we resolve the operators $\lambda^*, \mu^*, \gamma^*$ and δ^* into their real and imaginary parts, for a general linear viscoelastic solid. Following Biot (1962), the

operators γ^* and δ^* are approximated by elastic coefficients, i.e. $\gamma^* = \gamma,\ \ \delta^* = \delta$. Following Silva (1976), we write $\mu^* = \mu_R\left(1 + iQ_s^{-1}\right)$, and $\lambda^* + 2\mu^* = \left(\lambda_R + 2\mu_R\right)\left(1 + iQ_e^{-1}\right)$, where Q_e^{-1} and Q_s^{-1} are compressional specific attenuation and shear specific attenuation, respectively. Subscript *R* denotes the real parts of the corresponding quantities. Following Zwikker and Kosten (1949), Biot (1956b), Fatt (1959), Yew and Jogi (1976), and Murphy III (1982) relevant elastic parameters for water-saturated sandstone are chosen to be

$$\delta = 0.73787\times10^{-11}\left(dynes/cm^2\right)^{-1},\ \gamma = 0.889\times10^{-11}\left(dynes/cm^2\right)^{-1}$$

$$\mu_R = 0.922\times10^{11}\ dynes/cm^2,\ \lambda_R = 0.3032\times10^{11}\ dynes/cm^2.$$

$$\rho_f = 1.0\,gm/cm^3,\ \ K_n = 1.0\ dynes/cm^3,\ \ K_t = 0.5\ dynes/cm^3,$$

$$\beta = 0.23,\ m = 4.34,\ Q_e^{-1} = 0.04,\ \ Q_s^{-1} = 0.047,\ \frac{\eta}{\omega\chi} = 56.$$

Following Bullen (1963), the material constants of granite as elastic half-space are considered $\lambda = 2.238\times10^{11}\ dynes/cm^2,\ \mu = 2.992\times10^{11}\ dynes/cm^2, \rho = 2.66\,gm/cm^3.$

Using all the above numerical values and equations (12) and (13), the reflection and transmission coefficients $Z_1,\ Z_2, Z_3, Z_4$ and Z_5, given by (14), are computed for incident P and *SV* waves. The angle of incidence θ_0, is considered to be varying from normal incidence $\left(\theta_0 = 0°\right)$ to grazing incidence $\left(\theta_0 = 90°\right)$. We restrict the numerical computations for homogeneous case only.

(a) Incident P Wave

The amplitude ratios of reflected *P* waves are computed for the cases of Normal Stiffness (N-S), Transverse Stiffness (T-S) and Welded Contact (W-C) and are plotted against the angle of incidence ($0^o < \theta_0 < 90^o$) of *P* wave. The variations for N-S, T-S and W-C cases are shown in Figure 2 by black, blue and green curves, respectively. For N-S case, the amplitude ratio of reflected *P* wave is one at normal incidence. It decreases sharply to its minimum value 0.1776 at $\theta_0 = 46^o$. Thereafter, it increases sharply to its maximum value at grazing incidence of *P* wave. For T-S and W-C cases, it has value 0.24 at normal incidence and it first decreases to its minimum and then increases sharply to value one at grazing incidence. Comparing the different curves in Figure 2, the effect of imperfect boundary is observed significantly at all angles of incidence except grazing incidence. This effect is maximum at normal incidence.

The amplitude ratios of reflected *SV* waves are computed for the cases of Normal Stiffness (N-S), Transverse Stiffness (T-S) and Welded Contact (W-C) and are plotted against the angle of incidence ($0^o < \theta_0 < 90^o$) of *P* wave as shown in Figure 2. In each case, the amplitude ratio of reflected *SV* wave increases sharply to its maximum value and then decrease sharply. Comparing different curves in Figure 2, it is observed that the effect of imperfect boundary is significant at all angles of incidence except normal and grazing incidence.

The amplitude ratios of refracted P_{12}, P_{22} and P_{32} waves for N-S, T-S and W-C interfaces are plotted against the angle of incidence of *P* wave as shown in Figures 4 to 6. These amplitude ratios are also affected due to imperfect boundary at all angles except grazing incidence.

(b) Incident SV Wave

The amplitude ratios of reflected *P* and *SV* waves for N-S, T-S and W-C interfaces are plotted against the angle of incidence ($0^o < \theta_0 < 90^o$) of *SV* wave as shown in Figures 7 and 8, respectively. The variations of these amplitude ratios are oscillatory in nature. The comparison of different curves in these figures shows the effect of imperfect boundary on amplitude ratios of reflected *P* and *SV* waves at all angles of incidence in range except normal incidence.

The amplitude ratios of refracted P_{12}, P_{22} and P_{32} waves for N-S, T-S and W-C interfaces are plotted against the angle of incidence ($0^o < \theta_0 < 90^o$) of *SV* wave as shown in Figures 9 to 11. The comparison of the different curves in these figures also shows the significant effect of imperfect boundary on amplitude ratios of various refracted waves.

5. Figures

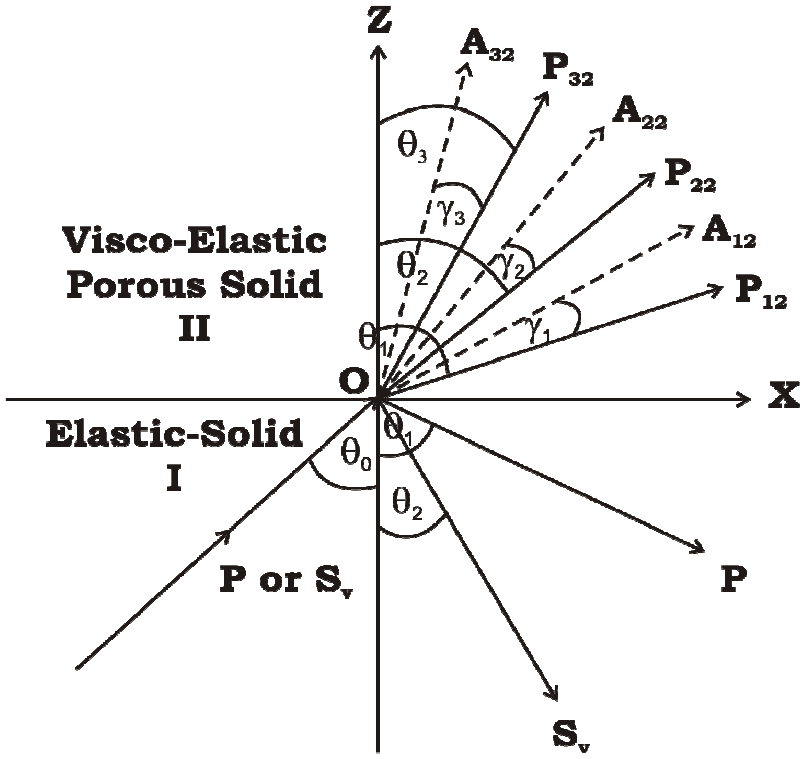

Figure 1: Geometry of the problem

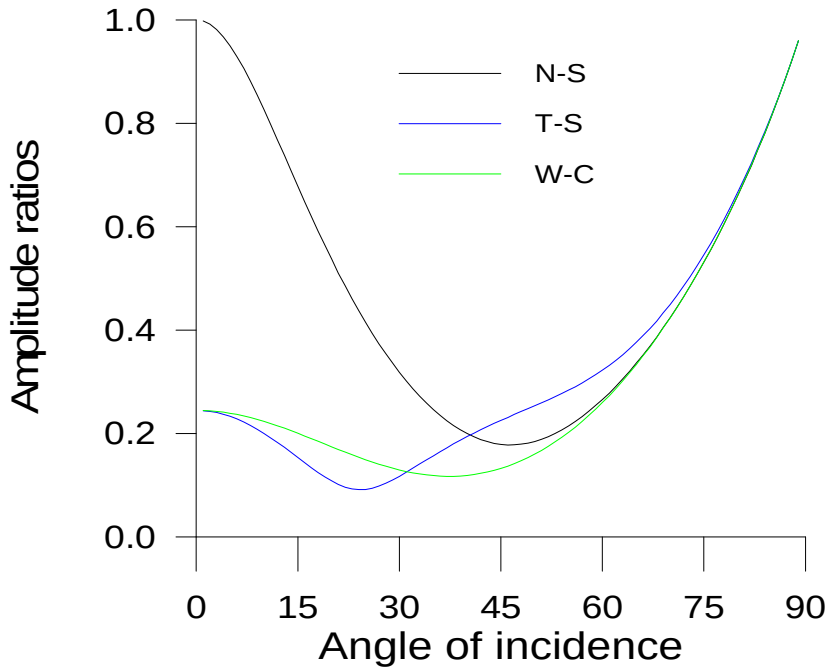

Figure 2: Variations of the amplitude ratios of reflected *P* wave against the angle of incidence of *P* wave for the cases of Normal Stiffness (N-S), Transverse Stiffness (T-S) and Welded Contact (W-C)

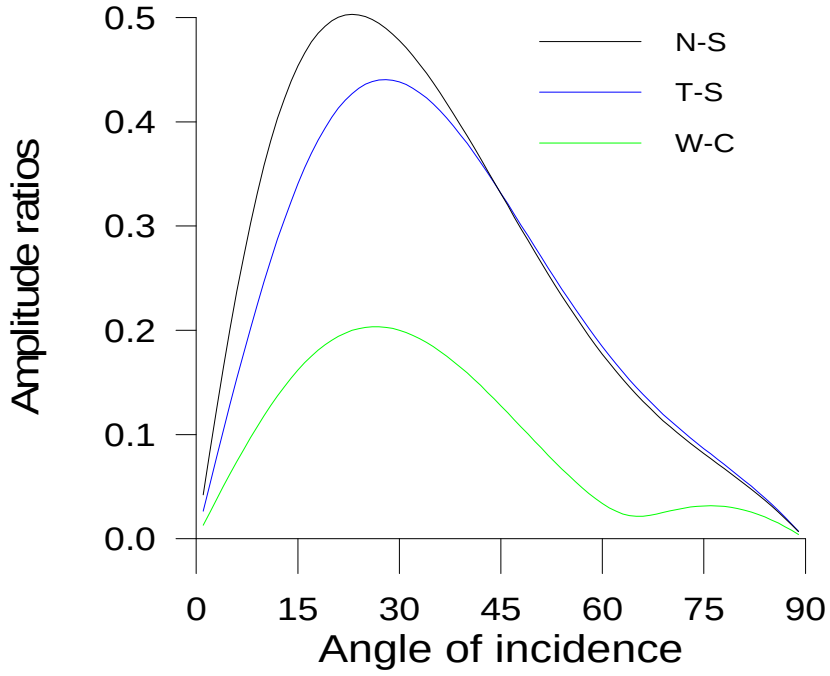

Figure 3: Variations of the amplitude ratios of reflected *SV* wave against the angle of incidence of *P* wave for the cases of Normal Stiffness (N-S), Transverse Stiffness (T-S) and Welded Contact (W-C)

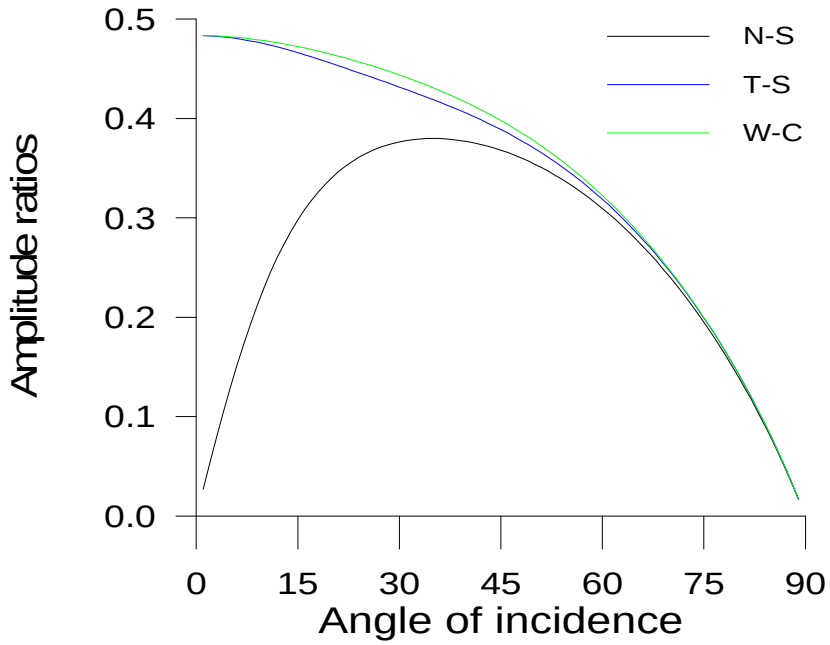

Figure 4: Variations of the amplitude ratios of reflected P_{12} wave against the angle of incidence of P wave for the cases of Normal Stiffness (N-S), Transverse Stiffness (T-S) and Welded Contact (W-C)

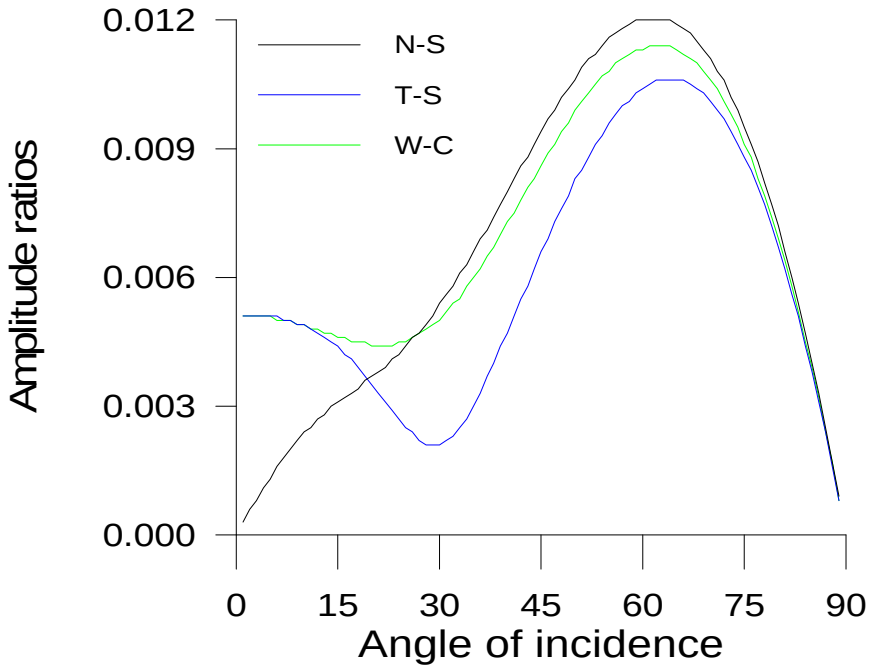

Figure 5: Variations of the amplitude ratios of reflected P_{22} wave against the angle of incidence of P wave for the cases of Normal Stiffness (N-S), Transverse Stiffness (T-S) and Welded Contact (W-C)

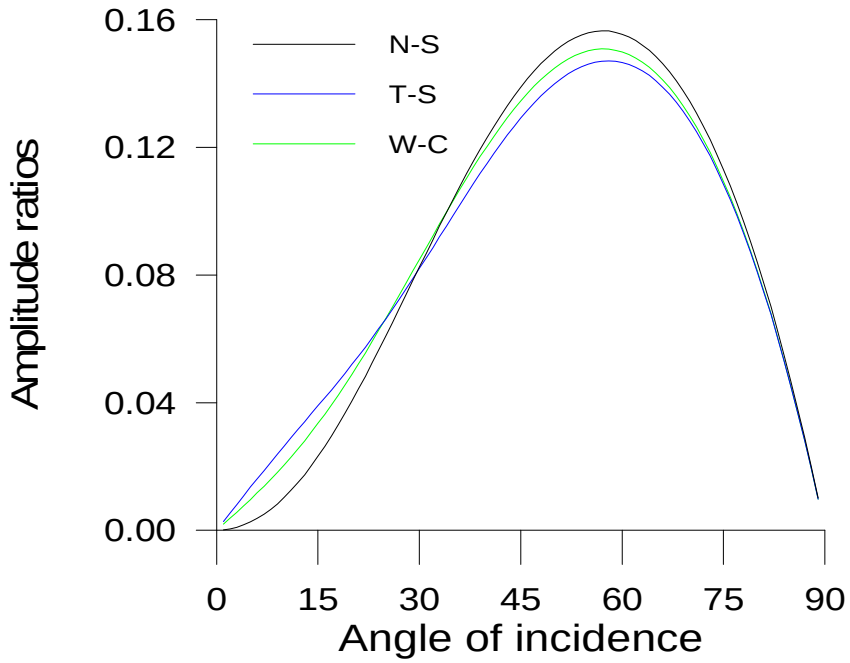

Figure 6: Variations of the amplitude ratios of reflected P_{32} wave against the angle of incidence of *P* wave for the cases of Normal Stiffness (N-S), Transverse Stiffness (T-S) and Welded Contact (W-C)

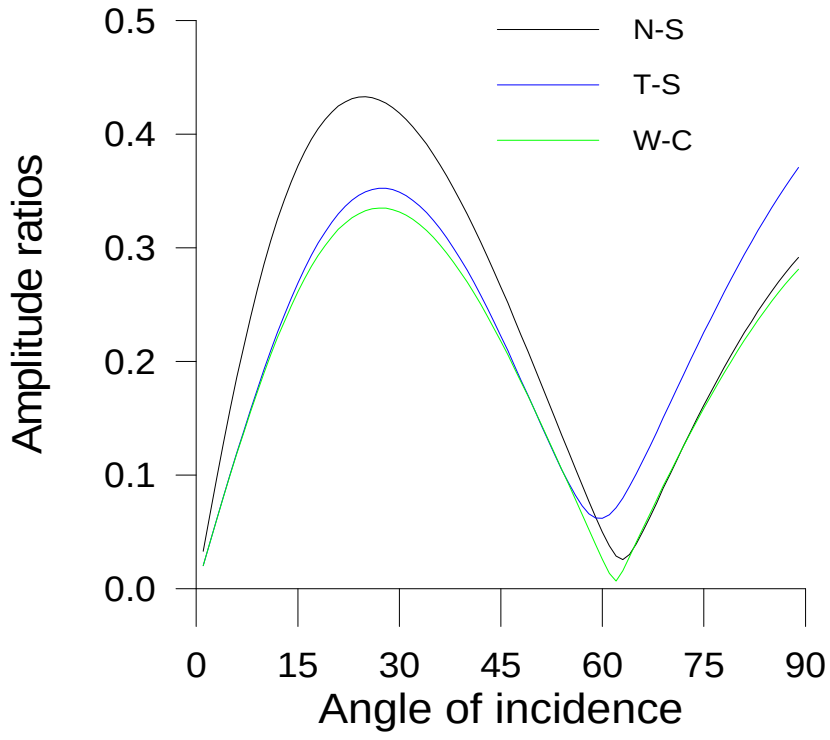

Figure 7: Variations of the amplitude ratios of reflected *P* wave against the angle of incidence of *SV* wave for the cases of Normal Stiffness (N-S), Transverse Stiffness (T-S) and Welded Contact (W-C)

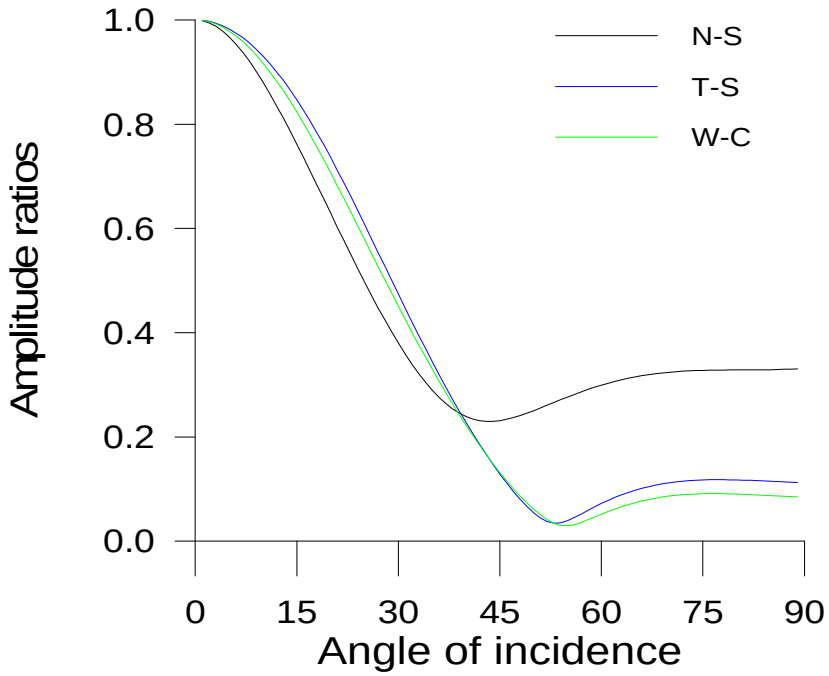

Figure 8: Variations of the amplitude ratios of reflected *SV* wave against the angle of incidence of *SV* wave for the cases of Normal Stiffness (N-S), Transverse Stiffness (T-S) and Welded Contact (W-C)

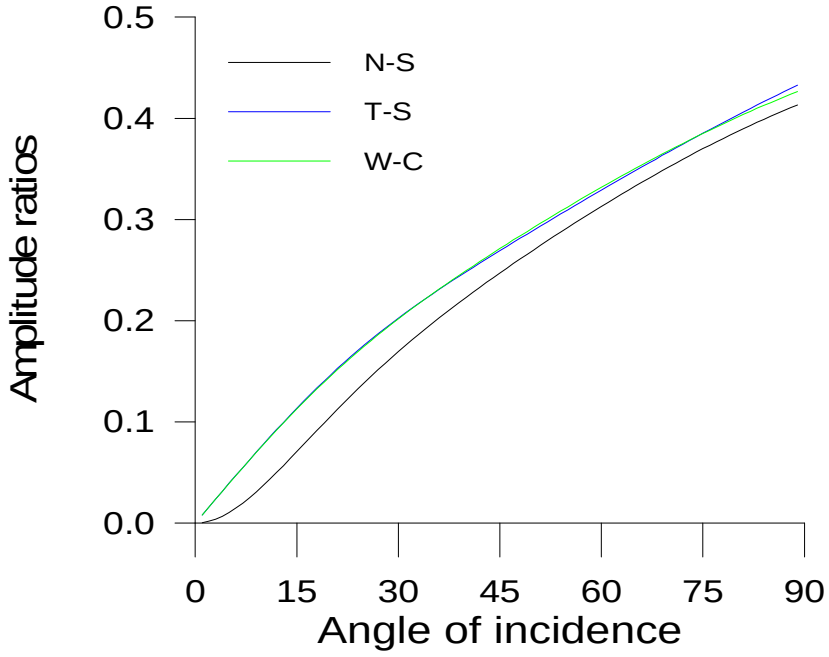

Figure 9: Variations of the amplitude ratios of reflected P_{12} wave against the angle of incidence of *SV* wave for the cases of Normal Stiffness (N-S), Transverse Stiffness (T-S) and Welded Contact (W-C)

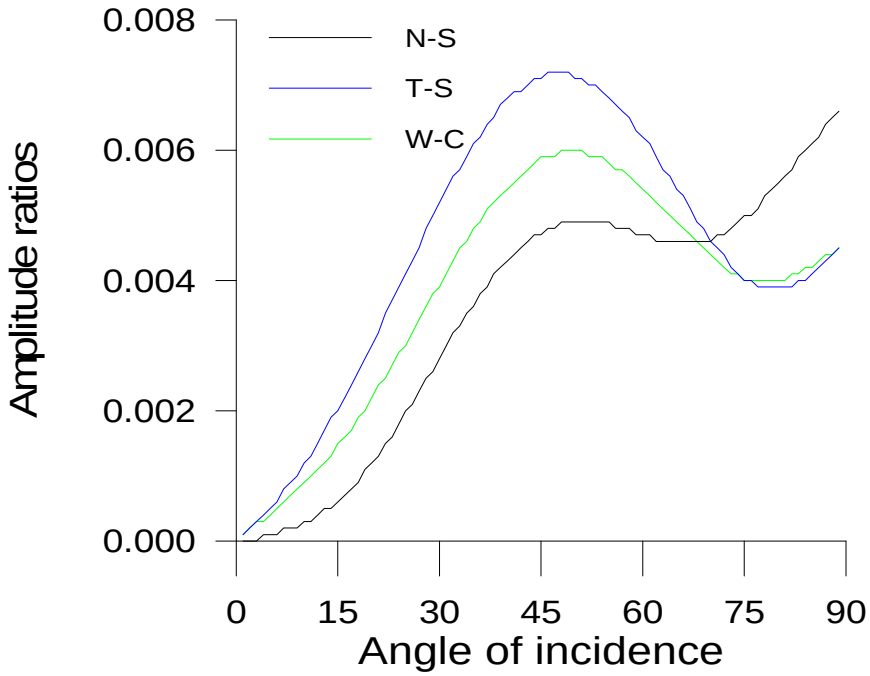

Figure 10: Variations of the amplitude ratios of reflected P_{22} wave against the angle of incidence of *SV* wave for the cases of Normal Stiffness (N-S), Transverse Stiffness (T-S) and Welded Contact (W-C)

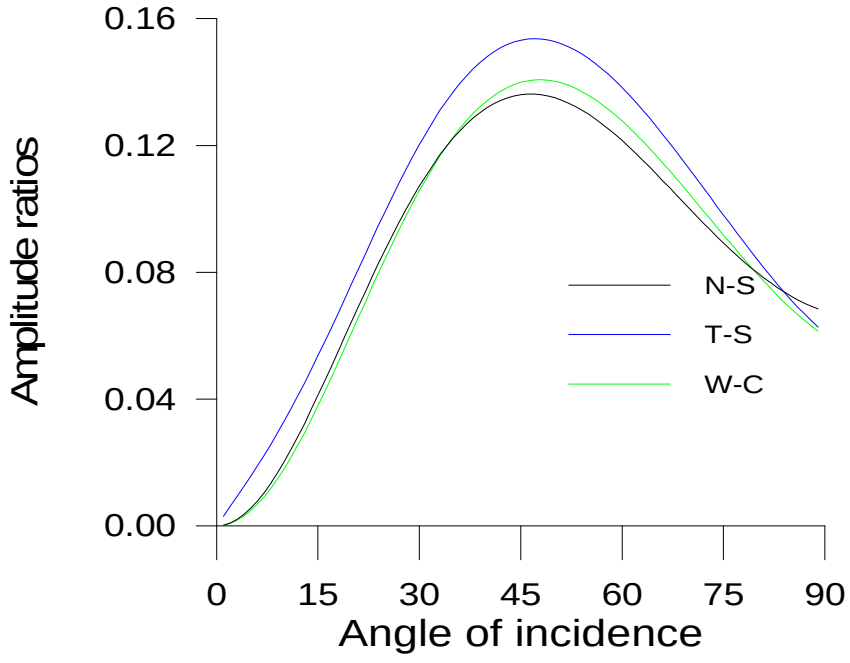

Figure 11: Variations of the amplitude ratios of reflected P_{32} wave against the angle of incidence of *SV* wave for the cases of Normal Stiffness (N-S), Transverse Stiffness (T-S) and Welded Contact (W-C)

6. Conclusion

Relations between reflection and transmission coefficients are obtained for incident of *P* and *SV* at an imperfect bonded interface between an elastic solid half-space and a viscoelastic porous solid half-space. Numerical values of these coefficients are computed for a particular model of the interface and shown graphically against the angle of incidence of *P* and *SV* wave for the cases of normal stiffness, transverse stiffness and welded contact. The amplitude ratio of refracted P_{22} wave is much smaller as compared to other reflected and refracted waves at all angles of incidence of *P* and *SV* waves. The amplitude ratios are affected significantly due to the presence of normal stiffness and transverse stiffness at each angle of incidence of *P* and *SV* wave.

References

[1] M.A. Biot, The theory of propagation of elastic waves in fluid-saturated porous solids, *J. Acoust. Soc. Am.*, 28(1956a), 168-191.

[2] M.A. Biot, Theory of deformation of a porous viscoelastic anisotropic solid, *J. Appl. Phys.*, 27(1956b), 459-467.

[3] M.A. Biot, Mechanics of deformation and acoustic propagation in porous media, *J. Appl. Phys.*, 33(1962), 1482-1498.

[4] R.D. Borcherdt, Reflection-refraction of general P and type-I S waves in elastic and anelastic solids, *Geophys. J. R. Astr. Soc.*, 70(1982), 621-638.

[5] I. Fatt, The Biot-Willis elastic coefficients for sandstone, *J. Appl. Mech.*, 26(1959), 296-297.

[6] W.F. Murphy III, Effects of partial water saturation in massilon-sandstone and vycor porous glass, *J. Acoust. Soc. Am.*, 71(1982), 1458-1468.

[7] M.D. Sharma and M.L. Gogna, Seismic wave propagation in a viscoelastic porous solid saturated by viscous liquid, *Pure Appl. Geophys.*, 135(1991), 383-400.

[8] M.D. Sharma, Rayleigh waves in dissipative poro-viscoelastic media, *Bull. Seismo. Soc. Am.*, 102(2012), 2468-2483.

[9] W. Silva, Body waves in layered anelastic solid, *Bull. Seismo. Soc. Am.*, 66(1976), 1539-1554.

[10] A.K. Vashishth and M.D. Sharma, Propagation of plane waves in poroviscoelastic anisotropic media, *Appl. Math. Mech.*, 29(2008), 1141-1153.

[11] C.H. Yew and P.N. Jogi, Study of wave motions in fluid-saturated porous rocks, *Acoust. Soc. Am.*, 60(1976), 2-8.

[12] C. Zwikker and C.W. Kosten, Sound Absorbing Materials, Elsevier Publishing Company, Inc., New York, 1949.